Electronic Supplementary Material (ESI) for ChemComm.

Supporting Information:

Pt modulation $NbSe_2$ with enhanced activity and stability: A new $Pt_3Nb_2Se_8$ compound for highly-efficient alkaline hydrogen evolution

Mengjia Luo,[†ab] Tong Wu,[†ab] Shumao Xu,[a] Ruiqi Wang,[c] and Fuqiang Huang[*abcd]

[a.] *State Key Laboratory of High Performance Ceramics and Superfine Microstructure, Shanghai Institute of Ceramics, Chinese Academy of Sciences, Shanghai 200050, P.R. China;*

[b.] *Center of Materials Science and Optoelectronics Engineering, University of Chinese Academy of Sciences, Beijing 100049, China;*

[c.] *State Key Laboratory of Rare Earth Materials Chemistry and Applications, College of Chemistry and Molecular Engineering, Peking University, Beijing 100871, P.R. China*

[d.] *CAS Centre for Excellence in Superconducting Electronic (CENSE), Shanghai 200050, China*

† These† These authors contributed equally: Mengjia Luo and Tong Wu

List of contents:

1. Experimental section.

Reagents. The following reagents were used: Nb (99.9%, Alfa Aesar), Pt (99.99%, ZhongNuo Advance Material (Beijing) Technology Co.), Se (99.9%, Sinopharm Chemical ReagentCo., Ltd). NaSe powder was produced by a liquid ammonia method.

Synthesis of $Pt_3Nb_2Se_8$ Single Crystals. Single crystals of $Pt_3Nb_2Se_8$ were synthesized by the solid-state reaction. A mixture of 1 mmol NaSe powder, 1 mmol Pt powder, 1 mmol Nb powder and 1 mmol Se powder was ground and loaded into carbon-coated fused silica tubes under an Ar atmosphere in a glovebox, which was flame-sealed under vacuum (10^{-3} mbar). The tubes were heated to 1323 K in 6 h and kept at the temperature for 25 h, then cooled to room temperature by turning off the furnace. Black fiber-shaped crystals were obtained by breaking the tubes.

Synthesis of $Pt_3Nb_2Se_8$ Powder. Powder of $Pt_3Nb_2Se_8$ was synthesized by solid-state reaction of stoichiometric amount of Pt, Nb and Se powders in a sealed carbon-coated fused-silica tube evacuated to 10^{-3} mbar. The tubes were heated to 1123 K in 6 h and kept at this temperature for 2 days. Then the furnace was turned off and the tube was cooled to room temperature.

Single-Crystal X-ray Crystallography. Suitable crystal was chosen to perform the data collections. Single crystal X-ray diffraction was performed on a Bruker D8QUEST diffractometer equipped with Mo *Kα* radiation. The diffraction data were collected at room temperature by the *ω*- and *φ*- scan methods. The crystal structure was solved and refined using APEX3 program. Absorption corrections were performed with the multi-scan method (ASDABS).[1]

Characterization. The single crystals of $Pt_3Nb_2Se_8$ were investigated with a JEOL (JSM6510) scanning electron microscope equipped with energy dispersive X-ray spectroscopy (EDXS, Oxford Instruments). Powder X-ray diffraction of the samples were collected on a Bruker D8QUEST diffractometer equipped with mirror-monochromated Cu *Kα* radiation (*λ*= 0.15406 nm). The patterns were recorded in a

slow-scanning mode with 2ϑ from 10° to 80° at a scan rate of 6°/min. Simulated patterns were generated by using the MERCURY program and CIF file of the refined single crystal structure. The morphology and elemental composition of powder sample were investigated with a JEM-2100F transmission electron microscope. Temperature variation of the resistance was measured using the standard four-probe technique with the Resistivity model and collected on a Physical Properties Measurement System (PPMS, Quantum Design). X-ray Photoelectron Spectroscopy (XPS) measurements were run on a Thermo-escalab 250Xi instrument.

Electrocatalytic measurement. The electrochemical experiments were carried out in a three-electrode cell with a CHI760E electrochemical workstation. The ink was prepared by dispersing 2 mg of the catalyst and 3 mg of acetylene black and 100 μL of 5 wt% Nafion solution in ethanol (900 μL) by sonication to form a homogeneous dispersion. Then, 100 μL of the dispersion was drop-casted onto a nickel foam (NF), leading to a catalyst loading of 2.5 mg cm^{-2}. During the electrochemical measurements, carbon rod and Hg/HgO electrode were used as the counter and reference electrodes, respectively. The KOH electrolyte was bubbled with N_2 for 0.5 h before HER test. The pH of 1 M KOH was measured by pH tester (Shanghai INESA). Polarization curves were recorded by linear sweep voltammetry (LSV) at a scan rate of 5 mV s^{-1} in the range of 0 to -0.6 V versus RHE. To estimate the electrochemically active surface area (ECSA) of the catalyst, cyclic voltammogram (CV) was tested by measuring double-layer capacitance (C_{dl}) between 0 to -0.1 V at 50-250 mV s^{-1} for HER. The Nyquist plots were measured with frequencies ranging from 100 kHz to 1 Hz at the η of 100 mV for HER, and the amplitude of 5 mV at a certain potential.

Electronic Structure Calculation. The electronic structures of $Pt_3Nb_2Se_8$ were calculated under first principle using the Projected Augmented Wave Method (PAW)[2] within the density functional theory (DFT) as implemented in the Vienna Ab Initio Simulation Package (VASP).[3-5] Generalized gradient approximation (GGA) and parameterized by Perdew-Burke-Ernzerhof (PBE)[6] version were used to describe the exchange correlation functional. The cutoff energy of plane wave basis was set to 320

eV. A Monkhorst-Pack k-point grid of 3×2×8 was used for Brillouin zone (BZ) sampling. The lattice parameters were fixed as the diffraction data during structural optimization, while the positions of atoms could relax until the atomic forces on each atom reduce less than 0.01 eV/Å. High-symmetry points in Brillouin zones (Γ, X, S, Y, Z, U, and R represent (0, 0, 0), (0.5, 0, 0), (0.5, 0.5, 0), (0, 0.5, 0), (0, 0, 0.5), (0.5, 0, 0.5), and (0.5, 0.5, 0.5)) were considered in our band structure calculation.

2. Supplementary figures.

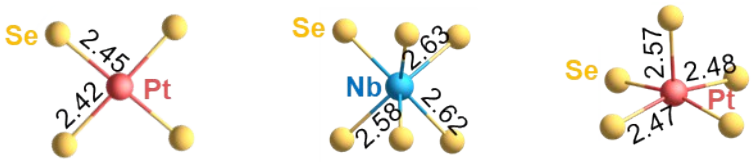

Fig. S1. The coordination environment of Pt and Nb.

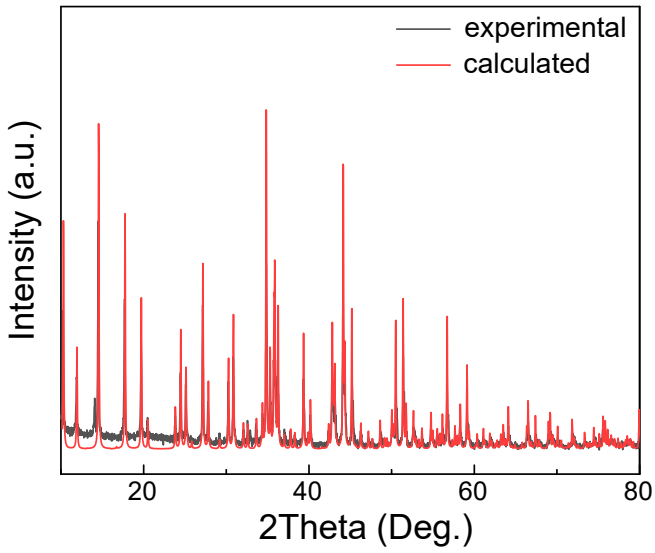

Fig. S2. The PXRD patterns of $Pt_3Nb_2Se_8$. The simulated patterns were generated (red line) based on the CIF files.

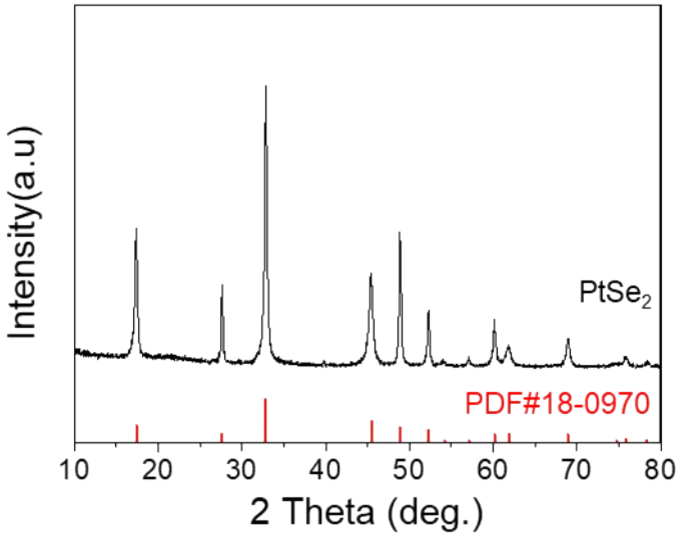

Fig. S3. The PXRD patterns (black line) and PDF card (red line) of $PtSe_2$.

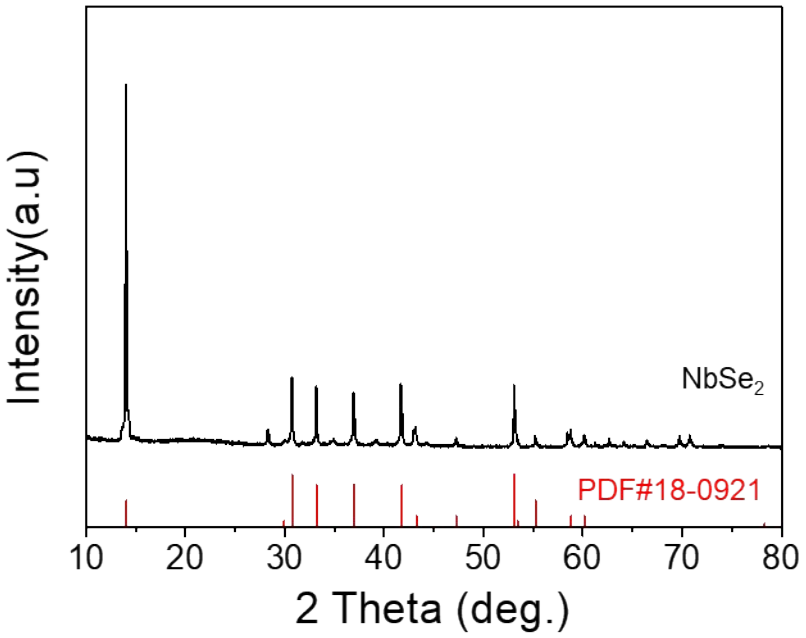

Fig. S4. The PXRD patterns (black line) and PDF card (red line) of $NbSe_2$.

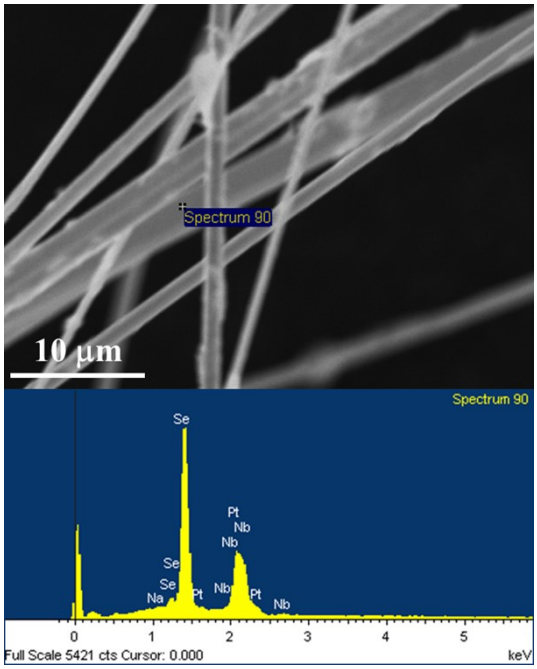

Fig. S5. The SEM image and EDX result of $Pt_3Nb_2Se_8$ crystal.

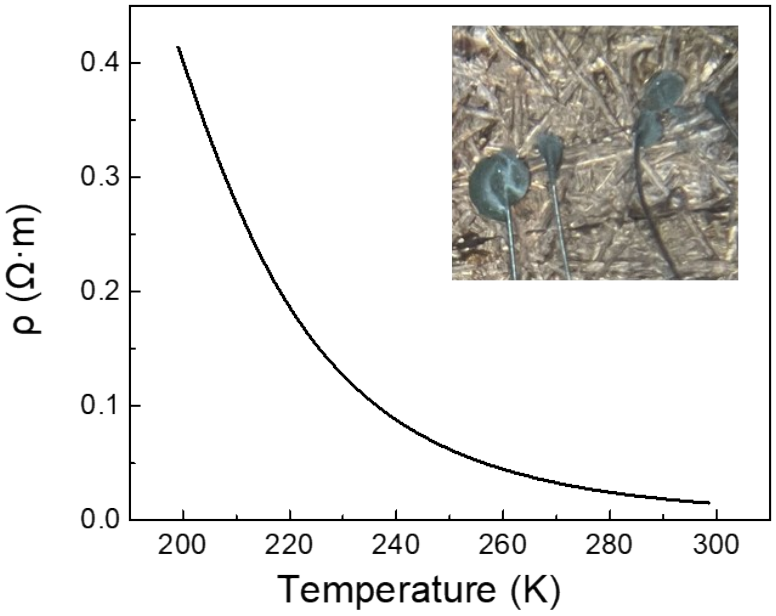

Fig. S6. Temperature dependence of electrical resistivity for $Pt_3Nb_2Se_8$.

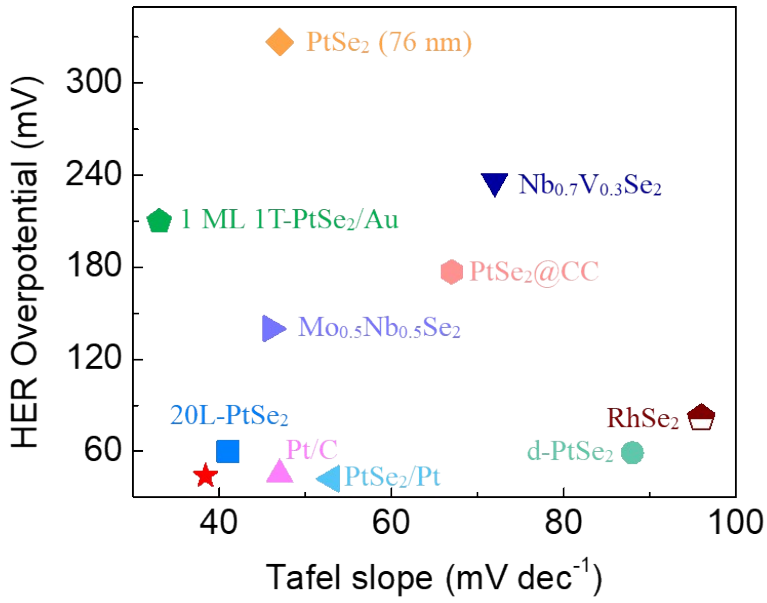

Fig. S7. Comparison of HER overpotential values and Tafel slope of $Pt_3Nb_2Se_8$, different $NbSe_2$, $PtSe_2$ or noble metal based electrocatalysts.

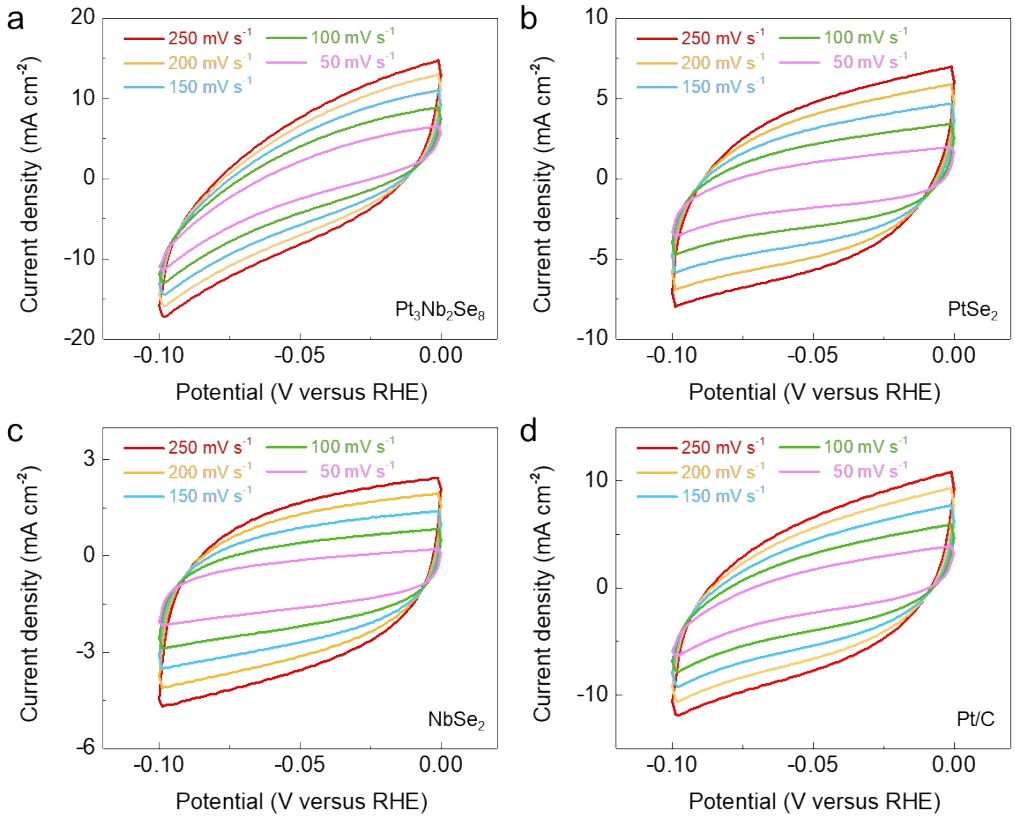

Fig. S8. Cyclic voltammetry (CV) curves of commercial $Pt_3Nb_2Se_8$, $PtSe_2$, $NbSe_2$, and Pt/C measured at -0.10-0.00 V vs. RHE with different scan rates from 50 to 250 mV/s.

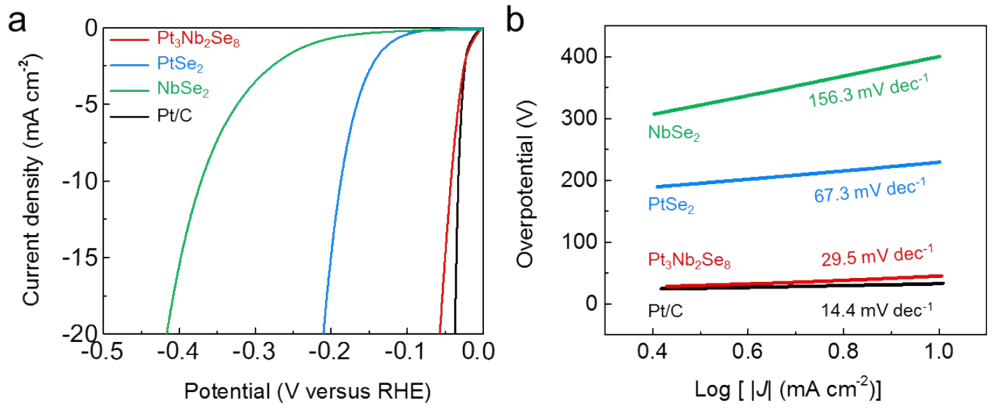

Fig. S9. HER performance in 0.5 M H_2SO_4. (a) Linear sweep voltammetry (LSV) curves and (b) corresponding Tafel plots of the $Pt_3Nb_2Se_8$, $PtSe_2$, $NbSe_2$, and commercial Pt/C.

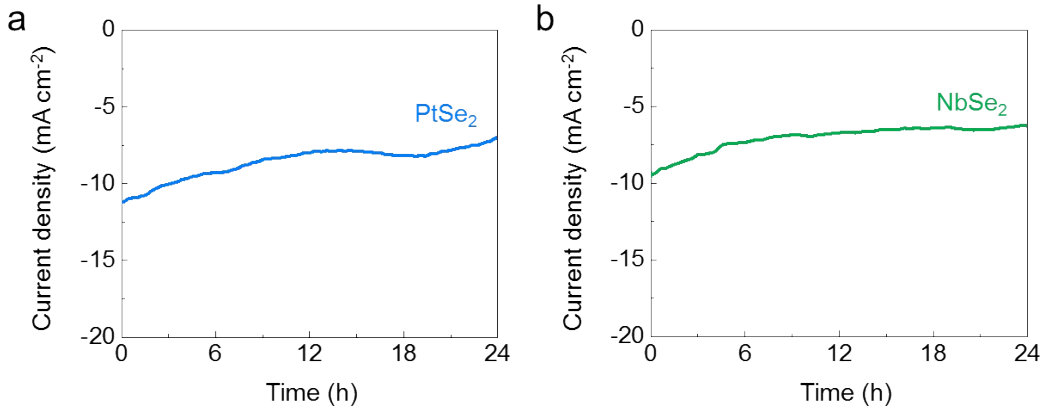

Fig. S10. The chronoamperometric test of (a) $PtSe_2$ and (b) $NbSe_2$ for 24 h at 10 mA cm^{-2}.

3. Supplementary tables.

Table S1. Crystal Data and details of the structure refinements for $Pt_3Nb_2Se_8$.

Chemical formula	$Pt_3Nb_2Se_8$
F_w (g·mol^{-1})	467.59
Crystal system	orthorhombic
Space group	*Pbam* (No. 55)
a (Å)	10.694(4)
b (Å)	15.017(6)
c (Å)	3.5633(15)

V (Å^3)	572.24(40)
Z	2
Crystal color	Black
ρ_c (g·cm^{-3})	8.142
μ (mm^{-1})	63.87
F(000)	591
Δρmax, Δρmin (e Å^{-3})	1.57, -2.24
R_1 [$I > 2\sigma(I)$]	0.027
wR_2 (all data)	0.039
GOF	1.07

[a] $R_1 = \sum||F_o| - |F_c||/\sum|F_o|$. [b] $wR_2 = \{\sum[w(F_o^2 - F_c^2)^2]/\sum[w(F_o^2)^2]\}^{1/2}$, $w = 1/[\sigma^2(F_o^2) + (0.1000P)^2]$, where $P = (F_o^2 + 2F_c^2)/3$.

Table S2. Atomic coordinates and isotropic displacement parameters (Å^2) of the $Pt_3Nb_2Se_8$ compound refined from single X-ray diffraction data recorded at room temperature.

atom	site	occ	x	y	z	U_{iso}*/U_{eq}
Pt01	4h	1	0.62679 (5)	0.21815 (4)	0.5	0.00661 (17)
Pt02	2b	1	0.5	0.5	0.5	0.0103 (2)
Nb03	4g	1	0.78940 (12)	0.11875 (9)	0	0.0065 (3)
Se04	4h	1	0.72878 (14)	0.49036 (9)	0.5	0.0088 (4)
Se05	4h	1	0.46025 (13)	0.34106 (10)	0.5	0.0071 (4)
Se06	4g	1	0.75254 (13)	0.28841 (10)	0	0.0081 (4)
Se07	4g	1	0.54778 (14)	0.11833 (10)	0	0.0079 (4)

Table S3. Atomic displacement parameters (Å^2) of $Pt_3Nb_2Se_8$.

atom	U^{11}	U^{22}	U^{33}	U^{12}	U^{13}	U^{23}
Pt01	0.0077 (3)	0.0076 (3)	0.0046 (4)	0.0006 (3)	0	0
Pt02	0.0092 (5)	0.0071 (5)	0.0145 (6)	-0.0007 (4)	0	0
Nb03	0.0065 (7)	0.0071 (7)	0.0060 (9)	0.0021 (6)	0	0
Se04	0.0113 (9)	0.0075 (8)	0.0076 (11)	0.0005 (7)	0	0
Se05	0.0092 (8)	0.0078 (8)	0.0044 (9)	0.0003 (6)	0	0
Se06	0.0106 (8)	0.0079 (8)	0.0057 (10)	-0.0013 (7)	0	0
Se07	0.0085 (8)	0.0106 (8)	0.0046 (10)	-0.0011 (7)	0	0

Table S4. Detailed bond lengths and angles (Å, °) of $Pt_3Nb_2Se_8$.

Pt01—Se06	2.4690 (12)	Pt02—Se04^{ii}	2.4508 (18)
Pt01—Se06^{i}	2.4691 (12)	Pt02—Se04	2.4508 (18)
Pt01—Se07^{i}	2.4769 (12)	Nb03—Se06	2.578 (2)
Pt01—Se07	2.4769 (12)	Nb03—Se07	2.584 (2)
Pt01—Se05	2.5648 (17)	Nb03—Se05^{iii}	2.6224 (16)
Pt01—Nb03^{i}	2.9028 (13)	Nb03—Se05^{iv}	2.6224 (16)
Pt01—Nb03	2.9028 (13)	Nb03—Se04^{v}	2.6323 (16)
Pt02—Se05^{ii}	2.4243 (17)	Nb03—Se04^{vi}	2.6323 (16)
Pt02—Se05	2.4244 (17)		
Se06—Pt01—Se06^{i}	92.37 (6)	Se05^{iii}—Nb03—Se04^{v}	132.83 (7)
Se06—Pt01—Se07^{i}	164.46 (5)	Se05^{iv}—Nb03—Se04^{v}	76.12 (5)
Se06^{i}—Pt01—Se07^{i}	85.72 (5)	Se06—Nb03—Se04^{vi}	135.44 (4)
Se06—Pt01—Se07	85.72 (4)	Se07—Nb03—Se04^{vi}	85.66 (5)
Se06^{i}—Pt01—Se07	164.46 (5)	Se05^{iii}—Nb03—Se04^{vi}	76.12 (5)
Se07^{i}—Pt01—Se07	92.00 (6)	Se05^{iv}—Nb03—Se04^{vi}	132.83 (7)
Se06—Pt01—Se05	94.05 (5)	Se04^{v}—Nb03—Se04^{vi}	85.20 (7)
Se06^{i}—Pt01—Se05	94.05 (5)	Se06—Nb03—Pt01	53.15 (3)
Se07^{i}—Pt01—Se05	101.46 (5)	Se07—Nb03—Pt01	53.29 (3)
Se07—Pt01—Se05	101.46 (5)	Se05^{iii}—Nb03—Pt01	83.22 (4)
Se06—Pt01—Nb03^{i}	109.65 (5)	Se05^{iv}—Nb03—Pt01	135.73 (6)
Se06^{i}—Pt01—Nb03^{i}	56.67 (5)	Se04^{v}—Nb03—Pt01	138.40 (6)
Se07^{i}—Pt01—Nb03^{i}	56.75 (5)	Se04^{vi}—Nb03—Pt01	85.24 (4)
Se07—Pt01—Nb03^{i}	109.55 (5)	Se06—Nb03—Pt01^{vii}	53.15 (3)
Se05—Pt01—Nb03^{i}	141.81 (2)	Se07—Nb03—Pt01^{vii}	53.29 (3)
Se06—Pt01—Nb03	56.67 (5)	Se05^{iii}—Nb03—Pt01^{vii}	135.73 (6)
Se06^{i}—Pt01—Nb03	109.65 (5)	Se05^{iv}—Nb03—Pt01^{vii}	83.23 (4)
Se07^{i}—Pt01—Nb03	109.55 (5)	Se04^{v}—Nb03—Pt01^{vii}	85.24 (4)
Se07—Pt01—Nb03	56.75 (5)	Se04^{vi}—Nb03—Pt01^{vii}	138.40 (6)
Se05—Pt01—Nb03	141.81 (2)	Pt01—Nb03—Pt01^{vii}	75.72 (4)
Nb03^{i}—Pt01—Nb03	75.73 (4)	Pt02—Se04—Nb03^{viii}	83.28 (5)
Se05^{ii}—Pt02—Se05	180.0	Pt02—Se04—Nb03^{ix}	83.28 (5)
Se05^{ii}—Pt02—Se04^{ii}	96.71 (5)	Nb03^{viii}—Se04—Nb03^{ix}	85.19 (7)
Se05—Pt02—Se04^{ii}	83.29 (5)	Pt02—Se05—Pt01	125.92 (6)

Se05^{ii}—Pt02—Se04	83.29 (5)	Pt02—Se05—Nb03^{x}	84.01 (5)
Se05—Pt02—Se04	96.71 (5)	Pt01—Se05—Nb03^{x}	130.50 (4)
Se04^{ii}—Pt02—Se04	180.0	Pt02—Se05—Nb03^{xi}	84.01 (5)
Se06—Nb03—Se07	81.35 (6)	Pt01—Se05—Nb03^{xi}	130.50 (4)
Se06—Nb03—Se05^{iii}	83.05 (5)	Nb03^{x}—Se05—Nb03^{xi}	85.60 (6)
Se07—Nb03—Se05^{iii}	134.21 (4)	Pt01—Se06—Pt01^{vii}	92.37 (6)
Se06—Nb03—Se05^{iv}	83.05 (5)	Pt01—Se06—Nb03	70.18 (4)
Se07—Nb03—Se05^{iv}	134.21 (4)	Pt01^{vii}—Se06—Nb03	70.18 (4)
Se05^{iii}—Nb03—Se05^{iv}	85.59 (6)	Pt01^{vii}—Se07—Pt01	92.00 (6)
Se06—Nb03—Se04^{v}	135.44 (4)	Pt01^{vii}—Se07—Nb03	69.97 (4)
Se07—Nb03—Se04^{v}	85.66 (5)	Pt01—Se07—Nb03	69.97 (4)

Symmetry codes: (i) *x*, *y*, *z*+1; (ii) -*x*+1, -*y*+1, -*z*+1; (iii) *x*+1/2, -*y*+1/2, *z*; (iv) *x*+1/2, -*y*+1/2, *z*-1; (v) -*x*+3/2, *y*-1/2, -*z*; (vi) -*x*+3/2, *y*-1/2, -*z*+1; (vii) *x*, *y*, *z*-1; (viii) -*x*+3/2, *y*+1/2, -*z*+1; (ix) -*x*+3/2, *y*+1/2, -*z*; (x) *x*-1/2, -*y*+1/2, *z*; (xi) *x*-1/2, -*y*+1/2, *z*+1.

Table S5. EDS results of $Pt_3Nb_2Se_8$.

Element	Weight%	Atomic%
Na K	0.21	0.96
Se L	47.21	62.82
Nb L	13.34	15.09
Pt M	39.24	21.13
Totals	100.00	100.00

Table S6. Performance comparison between $Pt_3Nb_2Se_8$ and $NbSe_2$, $PtSe_2$ based catalysts at a current density of -10 mA cm^{-2}.

Catalysts	Overpotential (mV)	Tafel slope (mV dec^{-1})	Ref.
$Pt_3Nb_2Se_8$	**44**	**38.4**	**This work**
Pt/C	45	47	*Adv. Mater.* **2020**, *1908521*
d-$PtSe_2$	59	88	*Adv. Energy Mater.* **2022**, *12, 2102359*
$PtSe_2$ (76 nm)	327	47	*Nano Energy* **2017**, *42, 26–33*
$PtSe_2$/Pt	42	53	*Angew.Chem.Int.Ed.* **2021**,*60,23388*
$Mo_{0.5}$ $Nb_{0.5}Se_2$	140	46	*ACS Nano* **2021**, *15, 5467−5477*
$Nb_{0.7}V_{0.3}Se_2$	236	72	*ACS Nano* **2022**, *16, 4278−4288*
$PtSe_2$@CC	177	67	*J. Mater. Chem. C* **2021**, *9, 9524–9531*
1ML 1T-$PtSe_2$/Au_2	210	33	*ACS Nano* **2019**, *13, 8442−8451*
20L-$PtSe_2$	60	41	*Angew.Chem.Int.Ed.* **2019**, *131, 7051*
$RhSe_2$	81	96	*Adv. Mater.* **2021**, *33, 2007894*

Reference：

1. G. Sheldrick, *Acta Crystallogr., Sect C.* 2015, **71**, 3-8.

2. P. E. Blöchl, *Phys. Rev. B.* 1994, **50**, 1953.

3. G. Kresse, Furthmüller, *J. Phys. Rev. B.* 1996, **54**, 11169-11186.

4. G. Kresse, Hafner, *J. Phys. Rev. B.* 1993, **47**, 558-559.

5. G. Kresse, Furthmüller, *J. Comput. Mater. Sci.* 1996, **6**, 15-50.

6. J. P. Perdew, K. Burke, *Phys. Rev. Lett.* 1996, **77**, 3865-3868.